

Drag Coefficient and Stanton Number Behavior in Fluid Flow Across a Bundle of Wing-Shaped Tubes

Andrej Horvat

Borut Mavko

Jožef Stefan Institute,
Reactor Engineering Division,
Jamova 39, SI 1001,
Ljubljana, Slovenia

Transient numerical simulations of fluid and heat flow were performed for eight heat exchanger segments with cylindrical and wing-shaped tubes in staggered arrangement. Their hydraulic diameters d_h were from 0.5824 to 3.899 cm for the cylindrical tubes, and from 0.5413 to 3.594 cm for the wing-shaped tubes. Based on the recorded time distributions of velocity $u_f(t)$ and temperature $T_f(t)$, time average Reynolds number \overline{Re} , drag coefficient \overline{C}_d , and Stanton number \overline{St} were calculated. In general, the drag coefficient and the Stanton number are smaller for the wing-shaped tubes than for the cylindrical tubes. However, with an increasing hydraulic diameter, these differences between both forms of tubes diminish. The time average values were further used to construct the drag coefficient and the Stanton number as polynomial functions $\overline{C}_d(d_h, \overline{Re})$ and $\overline{St}(d_h, \overline{Re})$.
[DOI: 10.1115/1.2241746]

Keywords: heat exchanger, tube shape, drag coefficient, Stanton number, numerical analysis

1 Introduction

Assessing drag and heat transfer between fluid flow and a structure in a heat exchanger is crucial to determine its operational parameters and performance already at the design stage. The assessment can be done by experimental testing (e.g., [1–4]) and by numerical calculations (e.g., [5–8]). Due to the nature of experimental work, an experimental investigation of all prototype geometries is not feasible. As an affordable substitute, numerical approaches and methods have been increasingly employed to simulate processes in heat exchangers in order to find new designs for emerging technological needs. Nevertheless, the direct numerical simulations of heat transfer processes in heat exchangers are still computationally too demanding. Therefore, significant simplifications, especially in the turbulence modeling and the wall effect treatment, are necessary.

Horvat and Mavko [9] proposed an alternative approach based on hierarchic modeling, in which the model and its computation are split onto two distinct levels. On the first level, transient three-dimensional numerical simulations of fluid and heat flow for geometry similar to a heat exchanger segment are performed. Based on the calculated three-dimensional velocity and temperature distributions, local values of the drag coefficient and of the heat transfer coefficient are determined. On the second level, an integral model [10], which uses the calculated local coefficients as input parameters, is applied to simulate heat transfer over a whole heat exchanger. As the computationally most demanding terms of

momentum and heat transport are determined on a separate level, the integral code is fast running, but still capable to accurately predict the heat flow for a whole heat exchanger.

Seeking an optimal geometry of heat exchanger tubes, we performed numerical simulations of fluid and heat flow for a larger number of heat exchanger segments with a different form of tubes. In this article, we would like to present computational results for wing-shaped tubes based on a NACA profile in a staggered arrangement. For comparison, the results of numerical simulations performed for cylindrical tubes are also presented. The numerical simulations cover laminar, transitional, as well as turbulent flow regime.

To adequately model fluid and heat flow phenomena in the heat exchanger segments, transient numerical simulations with a special near-wall treatment were performed. These calculations were used to obtain the time average values of the drag coefficient and Stanton number. Based on these values, we constructed \overline{C}_d and \overline{St} as polynomial functions of the Reynolds number and a geometrical parameter. For the most appropriate geometrical parameter, the hydraulic diameter d_h was chosen.

2 Geometrical Considerations

The numerical calculations were performed for a representative elementary volume (REV) of a tube bundle with staggered arrangement. The REV is colored grey in Fig. 1. The size and the shape of REV were selected after a fair amount of testing. We took under consideration errors arising from limiting the simulation domain, overall flow dynamics in the simulation domain, and needed computational resources. Based on the performed tests, it was concluded that in order to get representative data, it is more important to simulate longer time intervals than to enlarge the simulation domain.

In the case of cylindrical tubes, the diameter was 3/8 in. (9.525 mm). The calculations were performed for four geometries with different diagonal pitch-to-diameter ratio: $p/d = 1.125, 1.25, 1.5,$ and 2.0 . For each geometry, the REV height h was equal to the diagonal pitch p . The analysis was limited to the bundle arrangements where the pitch in the x -direction p_x is equal to the pitch in the y -direction p_y .

The geometries with the wing form of tubes were based on the NACA four-digit-series of profiles e.g., NACA0020, where the last two digits represent the thickness-to-chord ratio t/c [11]. In general, the NACA profile coordinates are calculated as

$$\frac{y}{c} = a_0 \left(\frac{x}{c}\right)^{1/2} + a_1 \left(\frac{x}{c}\right) + a_2 \left(\frac{x}{c}\right)^2 + a_3 \left(\frac{x}{c}\right)^3 + a_4 \left(\frac{x}{c}\right)^4 \quad (1)$$

For $t/c = 1/5$, the coefficients are given by Ladson et al. [11]

$$a_0 = 0.2969, \quad a_1 = -0.126, \quad a_2 = -0.3516 \\ a_3 = 0.2843, \quad a_4 = -0.1015 \quad (2)$$

To obtain a segment with the same fractions of the fluid phase and the solid structure as in the case of cylindrical tubes

$$V_{f,cyl} = V_{f,wing} \quad \text{and} \quad V_{s,cyl} = V_{s,wing}, \quad (3)$$

t/c was increased to $2/3$. Therefore, the ordinates y in function (1) were multiplied by $(2/3)/(1/5)$. Finally, the length of the chord c , and consequently, the size of the REV were determined from the requirement (3).

3 Simulation Details

The CFX 5.7 commercial code (ANSYS, Inc. [12]) was used to perform three-dimensional transient numerical simulations of air flow and heat transfer in REV. The tube walls in REV were treated as isothermal with the temperature $T_{wall} = 35^\circ\text{C}$. To allow disturbances to propagate over the geometrical limits of the simulation domain, the periodic boundary conditions were assigned in all three directions for all other boundaries. In order to consistently

Contributed by the Heat Transfer Division of ASME for publication in the JOURNAL OF HEAT TRANSFER. Manuscript received April 16, 2005; final manuscript received March 5, 2006. Review conducted by Sumanta Acharya.

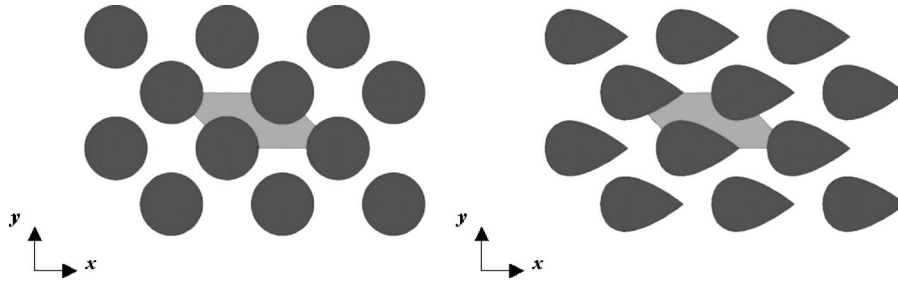


Fig. 1 Geometrical arrangement of heat exchanger structure for $p/d=1.25$; cylindrical (left) and wing (right) form

model the flow, periodicity had to be imposed on the transport equations in the streamwise direction.

As numerical results can be grid dependent, special care was taken to construct the numerical grids with sufficient resolution and uniformity. A basic criterion was the maximum nondimensional wall distance y^+ of the first layer of nodes. During the simulations, the maximum y^+ did not exceed the value of 2.0. The timestep for the transient calculations was based on an average time interval needed for a flow particle to pass the simulation domain

$$t_{\text{scale}} = \frac{2p_x}{u_f} \quad \text{and} \quad dt \leq \frac{t_{\text{scale}}}{80} \quad (4)$$

The details of the mathematical model and the validation of the numerical approach can be found in Horvat and Mavko [9].

4 Results

The transient numerical simulations of fluid and heat flow in REV were performed for the cylindrical and the wing-shaped tubes in the staggered arrangement (Fig. 1) with four different pitch-to-diameter ratios.

In order to extract relevant statistical values of physical variables, the volumetric average velocity

$$u_f(t) = \frac{1}{V_f} \int_{\hat{V}_f} u(t, x_i) dV \quad (5)$$

and the temperature

$$T_f(t) = \frac{1}{u_f(t)V_f} \int_{\hat{V}_f} u(t, x_i) T(t, x_i) dV \quad (6)$$

were recorded at each timestep after statistical steady-state flow conditions were reached. The length of the recording interval was set on a case-by-case basis, and it was at least 150 times longer than the time required for an average flow particle to travel the length of the simulation domain (4).

Using the obtained velocity distributions $u_f(t)$ and the temperature distributions $T_f(t)$, the Reynolds number

$$\text{Re}(t) = \frac{\rho u_f(t) d_h}{\mu} \quad (7)$$

the drag coefficient

$$C_d(t) = \frac{2\Delta p}{\rho u_f^2(t)} \left(\frac{A_f}{A_o} \right) \quad (8)$$

and the Stanton number

$$\text{St}(t) = \frac{\Delta T}{T_{\text{wall}} - T_f(t)} \left(\frac{A_f}{A_o} \right) \quad (9)$$

time distributions were calculated for each case. Further on, their time averages $\overline{\text{Re}}$, $\overline{C_d}$, and $\overline{\text{St}}$, and their standard deviations S_{Re} , S_{C_d} , and S_{St} were determined.

4.1 Drag Coefficient Functions. The time distributions of Reynolds number $\text{Re}(t)$ and drag coefficient $C_d(t)$ were obtained for both forms of tube cross sections. From the time distributions $\text{Re}(t)$ and $C_d(t)$, the statistical average values $\overline{\text{Re}}$ and $\overline{C_d}$ were calculated. Using the least-squares approximation, the calculated values enabled us to construct $\overline{C_d}$ for each form of tube cross sections as a polynomial function of Reynolds number $\overline{\text{Re}}$ and hydraulic diameter d_h . For the cylindrical form of tube cross sections, the function

$$\begin{aligned} \overline{C_d}(d_h, \overline{\text{Re}}) = & 0.2353 + 3.222 \cdot 10^{-10} d_h^{-4} + 1.348 d_h^{1/2} + 64.47 \overline{\text{Re}}^{-1} \\ & - 1.855 \cdot 10^{-5} \overline{\text{Re}} - 2.118 \cdot 10^{-9} \overline{\text{Re}}^2 \end{aligned} \quad (10)$$

was obtained. For the wing form of tube cross sections, we calculated the following function:

$$\begin{aligned} \overline{C_d}(d_h, \overline{\text{Re}}) = & -0.3020 + 1.825 \cdot 10^{-10} d_h^{-4} + 3.854 d_h^{1/2} + 2.875 \overline{\text{Re}}^{-1} \\ & - 6.518 \cdot 10^{-7} \overline{\text{Re}} - 7.158 \cdot 10^{-13} \overline{\text{Re}}^3 \end{aligned} \quad (11)$$

Figure 2 presents contour plots of the drag coefficient polynomials for the cylindrical (10) and for the wing (11) form of tube cross sections.

The comparison of the contour plots in Fig. 2 shows that the $\overline{C_d}$ function is much steeper for the wing form than for the cylindrical form of tube cross sections. For a given d_h , $\overline{C_d}$ monotonically decreases with $\overline{\text{Re}}$. If a value of $\overline{\text{Re}}$ is set, $\overline{C_d}$ has its minimum for a unique value of d_h . This value of the hydraulic diameter d_h is higher for the cylindrical form (~ 0.012 m) than for the wing form (~ 0.0075 m) of tube cross sections.

In Fig. 3, the drag coefficient functions (10) and (11) for the $p/d=1.125, 1.25, 1.5,$ and 2.0 are compared with the discrete values of $\overline{C_d}$ that were obtained from the time distributions (8). In general, the constructed polynomial functions (10) and (11), give a good approximation of the discrete values. Larger discrepancies exist only for $p/d=1.5$ at higher values of $\overline{\text{Re}}$.

In the laminar region, where the Reynolds numbers are a few hundred, the flow reaches steady-state conditions. Furthermore, $\overline{C_d}$ decreases with increasing $\overline{\text{Re}}$ much faster than in the turbulent region. The transition is usually marked with strong oscillations, where the flow periodically changes the direction and the spanwise motion of the fluid becomes important. As a consequence, $\overline{C_d}$ increases. The increase of $\overline{C_d}$ (Fig. 3) indicates that the transition to turbulence occurs at slightly lower $\overline{\text{Re}}$ for the cylindrical form

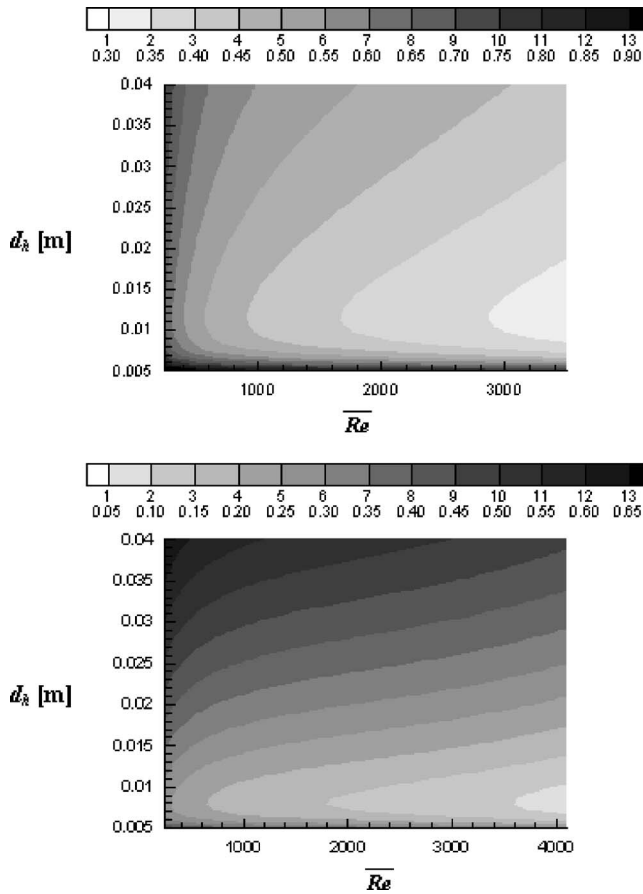


Fig. 2 Drag coefficient approximation functions (10) and (11) for (a) the cylindrical form and (b) the wing form

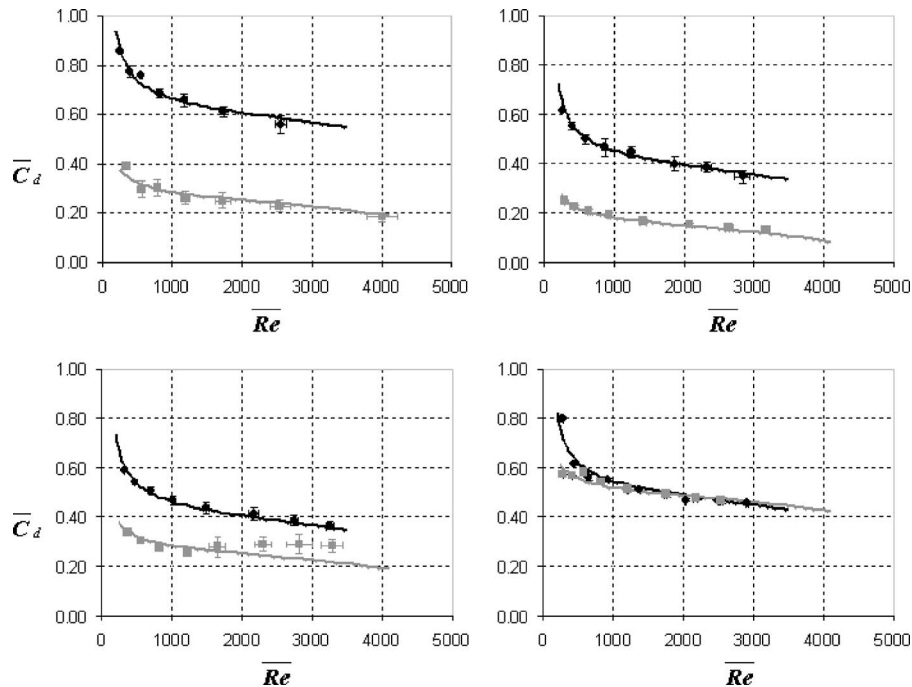


Fig. 3 Drag coefficient distribution for the cylindrical form (\blacklozenge) and the wing form (\blacksquare); (a) $p/d=1.125$, (b) $p/d=1.25$, (c) $p/d=1.5$, and (d) $p/d=2.0$

than for the wing form of tube cross sections. In the turbulent regime, \bar{C}_d changes at a much slower rate. Although, \bar{C}_d for the cylindrical form is in general larger than \bar{C}_d for the wing form, the difference with increasing d_h becomes negligible at the pitch-to-diameter ratio $p/d=2.0$ especially for larger values of Re .

Large oscillations were observed in the tube bundle with the wing form of tube cross sections at $p/d=1.5$. These oscillations are characterized by a separation of the boundary layer on the tube walls. The location of the separation triggers strong unsteady spanwise streams that increase \bar{C}_d . Similar behavior of the drag coefficient distributions can also be observed in the diagrams of the experimental data for the ellipsoidal form of tube cross sections recorded by Kays and London [2].

4.2 Stanton Number Functions. Using the recorded time distributions of Stanton number $St(t)$, the time averages \bar{St} were calculated for both forms of tube cross sections. From the calculated averages, the Stanton number approximation functions were determined with the least-squares method.

For the cylindrical tube cross sections, the function

$$\begin{aligned} \bar{St}(d_h, \overline{Re}) = & -0.02388 + 6.774 \cdot 10^{-12} d_h^{-4} - 0.01714 d_h^{1/2} \\ & + 6.553 (d_h / \overline{Re})^{1/2} + 2.090 \cdot 10^{-7} \overline{Re}^{-3} + 1.271 \overline{Re}^{-1/2} \\ & + 7.999 \cdot 10^{-6} \overline{Re} - 2.945 \cdot 10^{-13} \overline{Re}^3 \end{aligned} \quad (12)$$

was obtained, whereas for the wing form of tube cross sections the following function was calculated:

$$\begin{aligned} \bar{St}(d_h, \overline{Re}) = & -0.01863 + 1.331 \cdot 10^{-11} d_h^{-4} + 0.1185 d_h^{1/2} \\ & + 9.180 (d_h / \overline{Re})^{1/2} + 0.2078 \overline{Re}^{-1/2} + 3.271 \cdot 10^{-7} \overline{Re} \\ & - 2.530 \cdot 10^{-15} \overline{Re}^3 \end{aligned} \quad (13)$$

Figure 4 presents contour plots of the Stanton number polynomials for the cylindrical form (12) and for the wing form (13) of tube cross sections. For the range of Re under consideration, the amount of heat transfer crucially depends on the momentum transfer from the fluid flow to the structure walls. Therefore, the \bar{St}

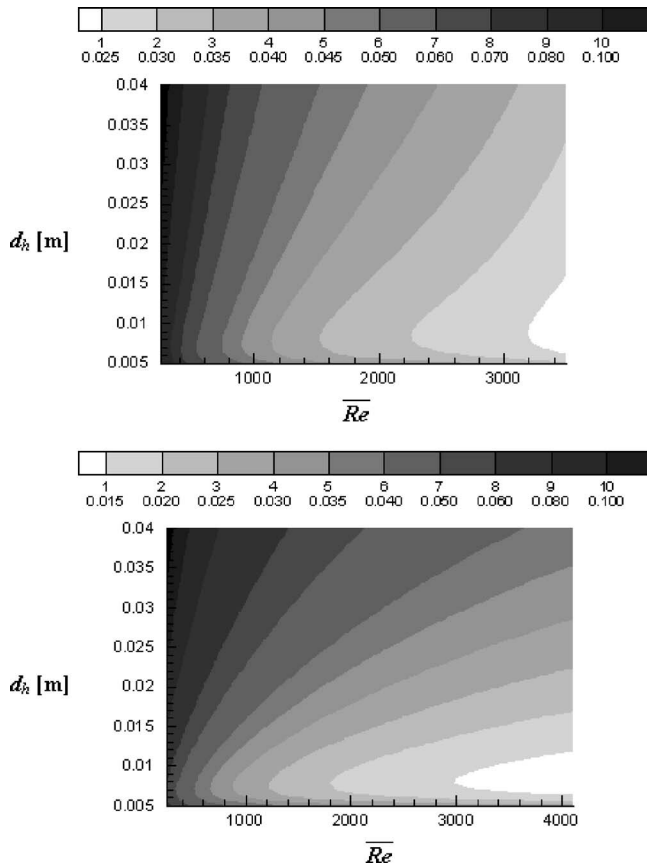


Fig. 4 Stanton number approximation functions (12) and (13) for (a) the cylindrical form and (b) the wing form

functions (Fig. 4) are similar to the \bar{C}_d functions (Fig. 2). The Stanton number monotonically decreases with increasing Re for any given d_h . This means that the flow velocity increases faster than the convective heat transfer from the isothermal walls to the fluid. Therefore, also the temperature $T_f(t)$ as defined by (6) decreases with increasing Re . The contour plots (Fig. 4) also show that if Re is set, St rapidly drops at small values of d_h and then gradually increases with the raising values of d_h .

In Fig. 5, the Stanton number functions (12) and (13) for the $p/d=1.125, 1.25, 1.5,$ and 2.0 are compared with the discrete values of St . The constructed polynomial functions (12) and (13) give a satisfactory approximation of the discrete values. Larger discrepancies can only be observed for the wing form of tube cross section at $p/d=1.5$ where the flow oscillations occur. In the laminar region, St decreases faster with increasing Re than in the turbulent region. The transitional behavior that is evident from the calculated values of \bar{C}_d (Fig. 3) shows almost no influence on the \bar{St} values. Figure 5 shows that \bar{St} is larger for the cylindrical than for the wing form of tube cross sections. Although, the difference is large for small d_h , it disappears at larger values of d_h .

5 Conclusions

Transient numerical simulations of heat transfer were performed for eight heat exchanger segments with the cylindrical and the wing-shaped tubes in the staggered arrangement. Their hydraulic diameters d_h were from 0.5824 to 3.899 cm for the cylindrical tubes, and from 0.5413 to 3.594 cm for the wing-shaped tubes. Based on the calculated results, the time distributions of Reynolds number $Re(t)$, drag coefficient $C_d(t)$, and Stanton number $St(t)$ were obtained. It is important to mention that we encounter much more complex physical behavior than it was reported in the available literature (e.g., [13–15]). Large flow oscillations and semi-stochastic motion of the flow in the spanwise direction were observed as the flow regime changes from laminar to turbulent.

Based on the recorded time distributions of velocity $u_f(t)$ and temperature $T_f(t)$, time average Reynolds number Re , drag coef-

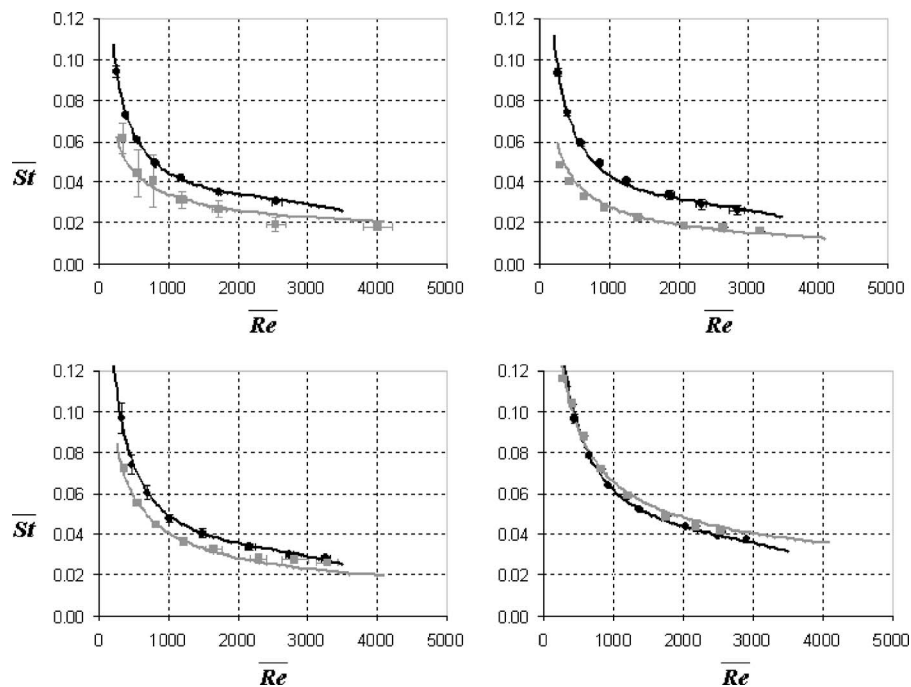


Fig. 5 Stanton number distribution for the cylindrical form (\blacklozenge) and the wing form (\blacksquare); (a) $p/d=1.125$, (b) $p/d=1.25$, (c) $p/d=1.5$, and (d) $p/d=2.0$

ficient \bar{C}_d , and Stanton number \bar{St} were calculated. The time average values \bar{Re} , \bar{C}_d , and \bar{St} were further used to construct the polynomial functions $\bar{C}_d(d_h, \bar{Re})$ and $\bar{St}(d_h, \bar{Re})$ for the cylindrical and the wing-shaped tubes. These polynomial functions are to be applied as input correlations in the integral model of a whole heat exchanger [10].

The calculated time average values \bar{Re} , \bar{C}_d , and \bar{St} also enabled us to draw some conclusions on the thermal performance of the cylindrical form and the wing form of tube cross sections. The drag coefficient \bar{C}_d as well as the Stanton number \bar{St} monotonically decrease with increasing \bar{Re} for any hydraulic diameter d_h . On the contrary, \bar{C}_d and \bar{St} exhibit minimum at a certain value of d_h for any given \bar{Re} . The minimum \bar{C}_d of the cylindrical form was found at $d_h \sim 0.012$ m, whereas for the wing form of tube cross sections the minimum \bar{C}_d was observed at $d_h \sim 0.0075$ m. In addition, the minimum value of \bar{St} was obtained at $d_h \sim 0.0075$ m for both sets of tested forms.

In general, the values of \bar{C}_d and \bar{St} are lower for the wing form in comparison to the cylindrical form of tube cross sections. Although, the differences are large at small d_h , they practically disappear at larger values of d_h . This allows us to conclude that the influence of different forms of bounding surfaces diminishes with increasing d_h .

Acknowledgment

A. Horvat gratefully acknowledges the financial support received from the Ministry of Higher Education, Science and Technology of the Republic of Slovenia for the project "Determination of morphological parameters for optimization of heat exchanger surfaces."

Nomenclature

A_f = $V_f/2p_x$, fluid flow cross section
 A_o = wetted surface
 a_i = coefficients of the NACA wing polynomial
 C_d = $2\Delta p/\rho u_f^2 (A_f/A_o)$, drag coefficient
 c = speed of sound, NACA wing chord length
 d = diameter
 d_h = $4V_f/A_o$, hydraulic diameter
 dt = timestep
 h = height of REV
 Pr = Prandtl number
 p = pitch between tubes, pressure
 Re = $\rho u_f d_h/\mu$, Reynolds number
 REV = representative elementary volume
 St = $\Delta T/(T_{wall} - T_f) (A_f/A_o)$, Stanton number
 T = temperature

t = time, NACA wing thickness
 t_{scale} = $2p_x/u_f$, average time needed for a flow particle to pass the simulation domain
 u = streamwise velocity
 V = volume
 V_f = fluid volume in REV
 y^+ = nondimensional wall distance

Greek

μ = dynamic viscosity
 ρ = density
 λ = thermal conductivity

Subscript/Superscript

f = fluid phase
 s = solid phase
 t = turbulence model variable
 $wall$ = wall conditions
 x = streamwise direction
 y = horizontal spanwise direction

References

- [1] Zhukauskas, A., 1987, "Convective Heat Transfer in Cross Flow," *Handbook of Single-Phase Convective Heat Transfer*, Wiley, New York.
- [2] Kays, W. S., and London, A. L., 1998, *Compact Heat Exchangers*, 3rd ed., Krieger, Malabar, Florida.
- [3] Kakac, S., 1985, *Heat Exchangers: Thermo-Hydraulic Fundamentals and Design*, 2nd ed., Hemisphere, New York.
- [4] Aiba, S., Tsuchida, H., and Ota, T., 1982, "Heat Transfer Around Tubes in In-Line Tube Banks," *Bull. JSME*, **25**, pp. 919–926.
- [5] Launder, B. E., and Massey, T. H., 1978, "The Numerical Prediction of Viscous Flow and Heat Transfer in Tube Banks," *ASME J. Heat Transfer*, **100**, pp. 565–571.
- [6] Antonopoulos, K. A., 1979, "Prediction of Flow and Heat Transfer in Rod Bundles," Ph.D. thesis, Mechanical Engineering Department, Imperial College, London, UK.
- [7] Beale, S. B., and Spalding, D. B., 1999, "A Numerical Study of Unsteady Fluid Flow in In-Line and Staggered Tube Banks," *J. Fluids Struct.*, **13**, pp. 723–754.
- [8] Barsamian, H. R., and Hassan, Y. A., 1997, "Large Eddy Simulation of Turbulent Crossflow in Tube Bundles," *Nucl. Eng. Des.*, **172**, pp. 103–122.
- [9] Horvat, A., and Mavko, B., 2005, "Hierarchic Modeling of Heat Transfer Processes in Heat Exchangers," *Int. J. Heat Mass Transfer*, **48**, pp. 361–371.
- [10] Horvat, A., and Catton, I., 2003, "Numerical Technique for Modeling Conjugate Heat Transfer in an Electronic Device Heat Sink," *Int. J. Heat Mass Transfer*, **46**, pp. 2155–2168.
- [11] Ladson, C. L., Brooks, C. W., Jr., and Hill, A. S., 1996, "Computer Program to Obtain Ordinates for NACA Airfoils," NASA TM 4741, Langley Research Center, Hampton, VA.
- [12] ANSYS, Inc., 2004, "ANSYS CFX 5.7.1 Documentation," www-waterloo.ansys.com/community/products.
- [13] Bejan, A., 1995, *Convection Heat Transfer*, 2nd ed., Wiley, New York.
- [14] Stanescu, G., Fowler, A. J., and Bejan, A., 1996, "The Optimal Spacing of Cylinders in Free-Stream Cross-Flow Forced Convection," *Int. J. Heat Fluid Flow*, **39**, pp. 311–317.
- [15] Matos, R. S., Vergas, J. V. C., Laursen, T. A., and Bejan, A., 2004, "Optimally Staggered Finned Circular and Elliptic Tubes in Forced Convection," *Int. J. Heat Fluid Flow*, **47**, pp. 1347–1359.